CrossMark

Hysteresis-free DC conduction in zinc oxide films with a conducting polymer counter electrode

Sharmistha Paul[1] · Paul G. Harris[2] · Ashwani K. Sharma[3] · Asim K. Ray[4]

Abstract

A conducting polymer, namely poly (3,4-ethylenedioxythiophene):poly(styrenesulfonate) (PEDOT:PSS) has been employed as an alternative metal counter electrode to study steady state charge conduction through a spin-coated 5.2 μm thick ZnO film in a sandwich structure on a fluorine doped tin oxide coated glass substrate. The room temperature current–voltage characteristics exhibit rectifying behaviour without hysteresis as the bias voltage is cycled between $\pm 10V$ for varying voltage sweep rate from 100 to 1000 mV/s. Thermionic emission is believed to be the dominant conduction mechanism at forward bias voltage $V \leq 2.5$ V whereas the space charge limited current conduction becomes effective in a higher voltage region $V > 2.5$ V. The barrier height (φ_b), ideality factor (n) and series resistance (R_s) are found to be strongly temperature dependent parameters showing the increase of ϕ_b and simultaneous decreases of n and R_s within the range of 218–298 K. The behaviour of the temperature dependent charge carrier mobility in the higher voltage region has also been discussed. The use of PEDOT:PSS is quite promising as an alternative to metal electrodes in semiconductor devices.

1 Introduction

The optical, electrical/electronic properties and stability of intrinsic conducting polymers are now considered to be sufficiently good for their use as alternatives to costly metal electrodes in the low cost production of high volume, large area, and flexible transparent electronic devices [1]. The *p*-type conducting polymer, polypyrrole has beeen used to fabricate a Schottky contact of high quality on *n*-type inorganic compound semiconductors devices such as indium phosphide (InP) [2]. In recent years, the conducting polymer poly (3,4-ethylenedioxythiophene):poly(styrenesulfonate) (PEDOT:PSS), which has HOMO and LUMO level at 5.2 and 3.5 eV respectively, is being increasingly employed as a hole injecting electrode in organic devices because of its high electrical conductivity which can be as large as 4380 S/cm, high optical transparency of nearly 90% and low cost large volume solution processability [3–5]. 200 nm thick spin coated PEDOT:PSS films are found to exhibit electrochromically fast response within 5 s for colour switching under the voltage cycling between ± 3.5 V [6]. Unlike indium tin oxide (ITO) electrodes, PEDOT:PSS electrode is environmentally friendly and the peak power efficiency of organic light emitting devices using multi-layered PEDOT:PSS electrode are reported to be 44% greater than those with ITO anodes without any outcoupling-enhancing structures [7]. The average field effect hole mobility is estimated to be 0.157 cm^2 V^{-1} s^{-1} for bottom gate organic thin film transistors using pentacene film as the main channel and electrohydrodynamic-printed PEDOT:PSS drain and source. This value is three orders of magnitude higher than the one obtained from similar pentacene transistors with vacuum deposited gold (Au) source and drain electrodes. Additionally, the resistances at PEDOT:PSS contacts is reported to be smaller than at Au contacts [8]. Semi-transparent, all plastic non-fullerene organic cells using film-transfer laminated PEDOT:PSS as the top electrode, are reported to exhibit 50% average visible transparency, meeting the requirement of the requirement of electricity generating windows and the power conversion efficiency is better than fullerene-based

✉ Asim K. Ray
  asim.Ray@rhul.ac.uk

[1] West Bengal State Council of Science & Technology, Vigyan Chetana Bhavan, 26/B, DD Block, Sector1, Salt Lake, Kolkata 700064, India

[2] Institute of Materials and Manufacturing, Brunel University, Uxbridge, Middlesex UB8 3PH, UK

[3] United States Air Force Research Laboratory, Space Vehicles Directorate, SE Kirtland AFB, NM 87117, USA

[4] Royal Holloway, University of London, Egham, Surrey TW20 0EX, UK

cells with similar thickness and transparency [9]. Highly flexible, stable, transparent supercapacitors have been fabricated using aerosol-jet sprayed sulfuric acid–polyvinyl alcohol (H$_2$SO$_4$/PVA) gel electrolytes as the binder and separator, sandwiched between two PEDOT:PSS electrodes. The devices with capacitance/areas of 0.84 mFcm^{-2} were found to be optically 80% transparent and able to endure 10,000 galvanostatic charge/discharge cycles at 20 A/m^2 [10].

Efforts have been made to produce good electrical contacts, Ohmic and Schottky, on zinc oxide (ZnO), a low toxicity, n-type oxide semiconductor having direct wide band gap of 3.37 eV and large electron affinity of 4.1–4.5 eV, for realising its many potential applications in flexible, transparent electronics [11]. 50 nm thick spin-coated PEDOT:PSS films on a single crystal ZnO (0001) is reported to have produced excellent Schottky junctions with a high rectifying ratio of 10^{10} at ± 2 V, low leakage current of 10 pA up to − 10 V and an ideality factor of 1.2. These results are comparable to those obtained for Schottky junctions with platinum and gold electrodes [12]. This type of Schottky diode can be employed as a highly sensitive ultraviolet detector with unity quantum efficiency. Values of 3.6×10^{14} cmHz$^{1/2}$W^{-1} and 10^3 have been estimated for normalised detectivity at 370 nm and the rejection ratio at zero bias condition, respectively [13]. The problem associated with the chemical activity between PEDOT:PSS electrodes and epitaxial grown ZnO films with O-polar surfaces can also be overcome by simply treating film surfaces with a silane-coupling agent of 3-aminopropyltriethoxysilane [14].

Low cost, room temperature printing techniques for depositing ZnO thin films on fluorine-doped tin oxide (FTO) substrate have been developed by us using commercially available zinc oxide (ZnO) nanoparticles. The performance of two terminal FTO/ZnO/Au memristors devices depends upon the voltage sweep rate, showing on–off ratios as large as 10^4 for 100 mV/s [15]. Multiple hopping between trap sites within the grain and grain boundary regions are believed to be responsible for charge transport through the FTO/ZnO/Au sandwich structure [16].

In this study, charge transport mechanisms of FTO/ZnO/PEDOT:PSS device have been determined through careful analysis of current–voltage (I–V) characteristics measured over a temperature range between 220 and 300 K when the bias voltage V was cycled between ± 10 V at three different rates of 100, 500 and 1000 mV/s. Comparison with FTO/ZnO/Au devices is made to evaluate the significance of using PEDOT:PSS as a metal alternative electrode material. Electrical parameters on Schottky diode using RF sputtered ZnO film on the ITO substrate and PEDOT:PSS have recently been reported over the limited bias voltage range of ± 1 V at higher temperatures varying between 302 and 373 K [17].

2 Experimental

Ultrasonically cleaned glass slides coated in fluorine-doped tin oxide (FTO) with a nominal surface resistivity of ~ 12 Ω/sq (supplied by VisionTek Systems, UK) were used for this investigation. The relatively less expensive FTO-coated substrates were chosen as the substrates for the ZnO film deposition because of their high conductivity, of the order of 2.3 Sm^{-1}, excellent chemical stability and 80% optical transparency within the visible region [18]. Thin films of ZnO were deposited on FTO-coated substrates by spinning a small volume of a 40 wt% dispersion of ZnO nanoparticles (< 130 nm) in ethanol (obtained from Sigma-Aldrich) at 250 and 2000 rpm sequentially for 15 and 60 s respectively. The solvent was then completely removed by oven drying the films in air at 120 °C for 15 min. The samples were annealed at 500 °C in air for 2 h through 30 min long temperature ramping from room temperature and back. The choice of the substrates depends upon the type of the measurement undertaken.

X-ray diffraction (XRD) patterns were acquired for the ZnO film on FTO substrates using a Bruker D8 Advance sweeping in the 2θ range of 5°–100°, with a step size of 0.02°/s using CuKα radiation of wavelength 0.15406 nm. Photoluminescence excitation and emission spectra of ZnO film on quartz substrates were measured at room temperature in the range from 250 to 800 nm by Horiba Jobin Yvon Fluorolog-3 spectrofluorometer with a pulsed 450 W Xenon lamp. Fourier transform infrared spectroscopy (FTIR) of the same film was recorded in the range of 400–4000 cm^{-1} at a resolution of 4 cm^{-1} by using Perkin Elmer Spectrum One FTIR spectrometer at room temperature.

For electrical characterisation, PEDOT:PSS polymer (Orgacon 3400, Agfa Speciality Products) was used as the top electrode of the 5.2 μm thick ZnO film in a sandwich configuration with FTO as the bottom electrode. PEDOT:PSS was spin-coated at 1000 rpm for 60 s on annealed ZnO films. The solution processing method of depositing the PEDOT:PSS electrode was chosen in order to avoid the possible formation of interfacial trap states. A Keithley 617 electrometer and an Oxford Instruments constant temperature liquid nitrogen cryostat were used in a microprocessor controlled measuring system to record steady state current–voltage characteristics for ZnO sandwich devices in vacuum of 10^{-4} mbar over the temperature range of 218–298 K. The voltage was applied to the sample through the PEDOT:PSS electrode from − 10 to + 10 V with scan rate 500 mV/s keeping the FTO electrode grounded.
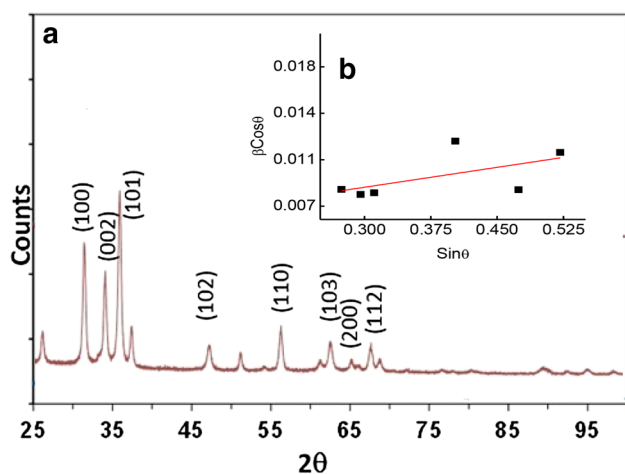
3 Results and discussion

Figure 1 shows the XRD pattern of the annealed ZnO spun film on FTO substrates. The peaks at 31.81°, 34.41°, 36.24°, 47.51°, 56.62°, 62.86°, 66.40°, 69.10° and 72.55° are identified with diffraction at (100), (002), (101), (102), (110), (103), (200) (112) and (004) planes because of their agreement with the reference values of JCPDS (36-1451). The intensity ratio $I_{(002)}/I_{(101)}$ is estimated to be nearly 0.5 which is close to the typical value of 0.44 for the bulk hexagonal wurtzite structure. A plot in the inset of Fig. 1 of $\beta\cos\theta$ as a function of $\sin\theta$ is found to be linear showing the validity of the Williamson–Hall equation in the form [19]:

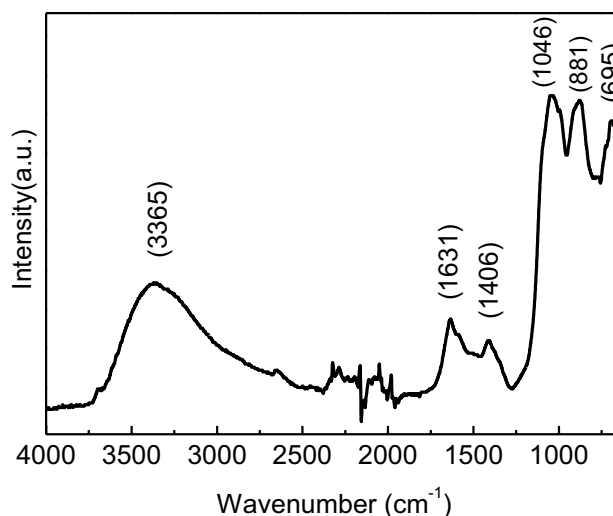$$\beta\cos\theta = \eta\sin\theta + \frac{\lambda}{D} \tag{1}$$

where β is the angular line width of half maximum intensity at the Bragg angle θ and $\lambda = 0.1540$ nm. Values of 28.36 nm and 0.01 are found for the average crystallite size D and the strain η from the intercept and the slope of the linear plot. These XRD results indicate the formation of an improved structure of ZnO films over ones recently reported for chemical bath deposited ZnO films [20]. The intensity ratio $I_{(002)}/I_{(101)}$ of 0.70 is considerably higher while a value of 22 nm for the average crystallite size D is smaller than the respective values obtained in the present investigation.

Figure 2 presents the mid-infrared regime FTIR spectrum for the annealed ZnO film between 1000 and 4000 cm^{-1}. The broad peak around 3365 cm^{-1} corresponds to the OH stretching vibration, implying the possible presence of residual hydroxyl ions in the ZnO film. The occurrence of this peak at a similar position has been reported for the ZnO film, newly synthesised by a wet chemical method using
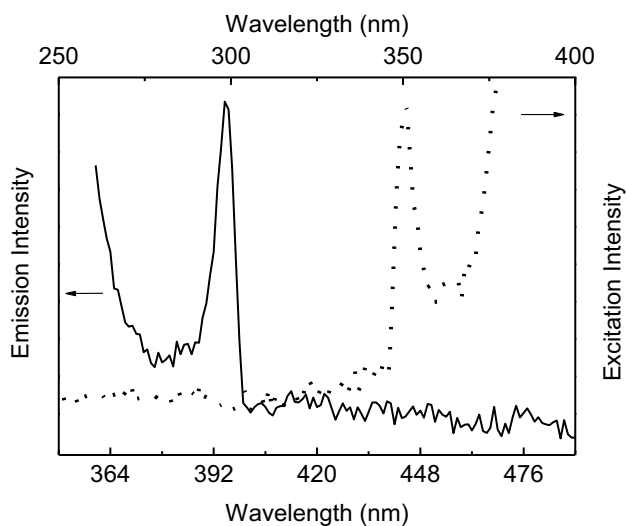
Fig. 2 FTIR spectra of annealed ZnO film on FTO coated glass slide

triethanolamine as a mild base [21]. The presence of two peaks at 1631 and 1406 cm^{-1} may be attributed to asymmetric and symmetric C–O stretching. The peaks at 881 and 695 cm^{-1} are due to Zn–O stretching [22].

The room temperature photoluminescence (PL) emission and excitation spectra of annealed ZnO film are shown in Fig. 3. The observation of a strong luminescence peak at 395 nm corresponding to 3.14 eV in the UV region of the emission spectra may be identified with near band energy emission and is in agreement with the value reported for ultrasonic spray pyrolysis deposited ZnO films on an FTO substrate [23]. The origin of this peak is usually attributed to the recombination of free excitons through exciton–exciton

Fig. 1 **a** XRD pattern of annealed ZnO film on FTO coated glass slide. **b** Plot of William-Hull line for the sample

Fig. 3 Photoluminescence spectra of annealed ZnO film: emission (solid line). Excitation spectra (broken line). Arrows show the relevant axes

collision process associated with the transition over the wide direct band gap of ZnO from the ground state to the continuum state [24]. No pronounced peak was found to have occurred in the visible range of the emission spectrum. This absence implies the formation of high crystal quality of ZnO films without the significant presence of oxygen vacancies [25]. The PL excitation spectrum is also recorded at the emission wavelength of 395 nm. The occurrence of the sharp band edge peak at 351 nm of the excitation spectrum may be considered as evidence of good crystalline and high purity synthesized ZnO nanoparticles. The presence of this strong absorption peak at 351 nm is considered to be blue-shifted relative to the peak at 373 nm for the bulk ZnO corresponding to a small increase of the band gap to 3.53 eV from the bulk value of 3.32 eV [26].

Figure 4a presents a set of reproducible room temperature current–voltage (I–V) curves of a FTO/ZnO/PEDOT:PSS structure as depicted in the top inset for one complete cycle between ± 10 V, as bias voltage V was swept in both forward and reverse directions through 0 V at three different sweep rates namely 100, 500 and 1000 mV/s respectively. The
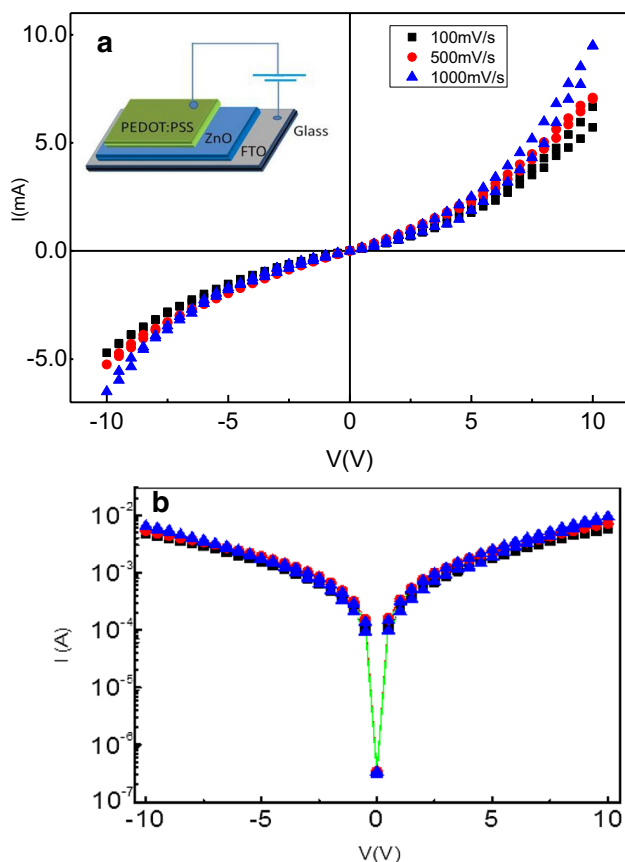
Fig. 4 **a** One complete cycle of I–V measurement of FTO/ZnO/PEDOT:PSS at different voltage sweep rates. Insets showing the device sandwich structure. **b** Plot of I–V on a logarithm–linear scale for the same device

magnitude of current in both bias directions is three orders higher than one reported for the similarly fabricated FTO/ZnO/Au device which showed multi-level conducting states in their (I–V) with large on–off ratios [15]. This implies that the PEDOT:PSS is more efficient in charge injection into the ZnO film than the Au electrode. The semi-logarithmic plot of I–V characteristics in Fig. 4b clearly indicates the absence of hysteresis for the measured sweep rates. The self-healing breakdown which is regarded as being responsible for existence of multi-level resistance states in the I(V) characteristics for the structure with an Au counter electrode seems not occur in FTO/ZnO/PEDOT:PSS device [27]. Further, the current I is found to have increased linearly at bias voltage V ≤ 1 V for all three sweep rates. However, the dependence of I on V becomes non-linear for V > 1 V. The voltage-dependent rectification ratio is found to lie within two orders of magnitude for different voltage sweep rates for the device. For the voltage region higher than 2.5 V, m is found to vary between 1.5 and 2, indicating that space-charge limited current (SCLC) conduction is occurring, where traps play a major role in controlling performance [28]. Values of m do not show significant variation with the sweep rates. The dependence of current on applied bias and its rectifying nature demonstrate that the PEDOT:PSS layer is behaving as a non-interacting conductive electrode for this device.

Electrical parameters such as barrier height (ϕ_b), ideality factor (n), series resistance (R_s) for Schottky contact between ZnO/PEDOT:PSS may be evaluated by applying thermionic emission theory in lower voltage region I (0–2.5 V). Therefore, for the applied voltage V > 3kT/q, the forward bias current at temperature T can be expressed as [29]:

$$I = I_s \left[\exp\left(\frac{q(V - IR_s)}{nkT} \right) - 1 \right] \tag{2}$$

where I_s, R_s, q, k and n are reverse saturation current, series resistance, elementary charge, Boltzmann constant and ideality factor, respectively. The reverse saturation current I_s is written in following form:

$$I_s = AA * T^2 \exp\left(\frac{-q\phi_b}{kT} \right) \tag{3}$$

where A is the active contact area (110×10^{-6} m²), A* is the Richardson constant, which has a theoretical value of 32 A cm⁻² K⁻² for ZnO [30] and ϕ_b is the Schottky barrier height. The value of I_s is obtained from the extrapolated intercept of ln I versus V plot (Fig. 5) with the current axis for V = 0 V. The calculated barrier heights ϕ_b at zero bias for different temperatures (298–218 K) are obtained within the range of 0.29–0.19 eV. The expected barrier height at a ZnO/PEDOT:PSS junction is 0.7 eV as the HOMO level of
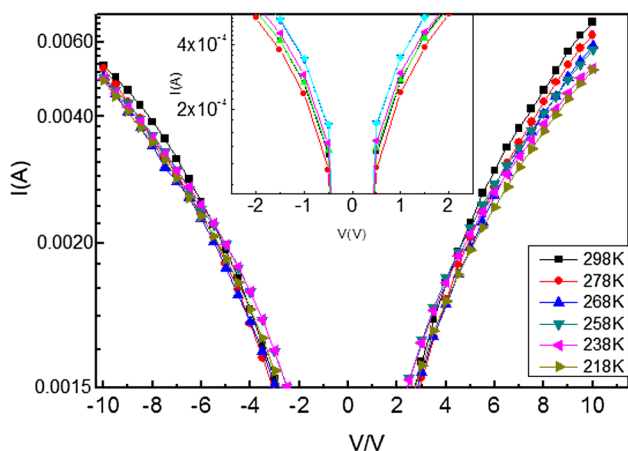
Fig. 5 Semi logarithm plots of *I–V* curves of FTO/ZnO/PEDOT:PSS device at different temperatures (218–298 K) between ± 10 V at 500 mV/s voltage sweep rate. Inset show *I–V* curves in lower voltage region (0–2.5 V)

Fig. 6 Variation of d*V*/dln(*I*) with *I* for FTO/ZnO/PEDOT:PSS device at different temperatures in forward bias. Inset shows variation of *n* with temperature

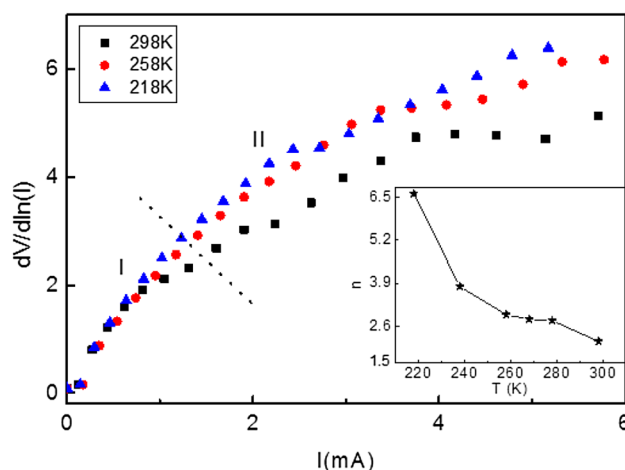PEDOT:PSS is at 5.2 eV which is within the band gap of ZnO forming a Schottky junction at this interface.

The ideality factor (*n*) and series resistance (R_s) of Schottky contacts can be obtained from following equations using the Cheung method [31]:

$$\frac{dV}{d(\ln I)} = \frac{nKT}{q} + IR_s \qquad (4)$$

$$H(I) = V - \left(\frac{nkT}{q}\right)\ln\left(\frac{I}{AA * T^2}\right) \qquad (5)$$

$$H(I) = n\phi_b + IR_s \qquad (6)$$

Figure 6 shows variation of d*V*/d(ln*I*) versus *I* at different temperatures from which the value of *n* can be obtained from the intercept at the zero current axis equating to (*nkT/q*) in a linear fit of lower voltage region I. The value of *n* is observed from the inset of Fig. 6 to decrease from 6.6 at 218 K to 2.2 at 298 K. A similar pattern of variation of *n* from 7.55 to 1.77 is observed for Pd/ZnO Schottky barrier diodes as T is varied from 60 to 300 K [32]. These values are higher than the ideal value of *n* = 1–2 for homogenous ZnO p-n junctions [33, 34]. Two different possible mechanisms are believed to be responsible depending upon the temperature: (i) generation recombination for T ≤ 260 K and (ii) thermionic emission from 260 K < T ≤ 300 K. However other factors that may contribute to the deviation of n from unity are current leakage effects, a lack of free-carrier concentration at low temperatures, parasitic rectifying junctions within the device and Schottky barrier inhomogeneity in the junction area [35]. Parameter *H* (*I*) can be calculated using '*n*' in Eq. 5. Figure 7 shows variation of *H*(*I*) with current (*I*) at three temperatures and the values of ϕ_b and R_s have

been estimated from the slope and intercept of the linear fit, respectively.

Figure 8 shows the variation of R_s and ϕ_b with temperature T for FTO/ZnO/PEDOT:PSS Schottky junctions. R_s, the important parameters of electrical characterization plays a crucial role of non-ideal behaviour of forward bias current due to the presence of an interface layer between ZnO and the polymer. The decrease in R_s with an increase in temperature may be due to barrier modification under the influence of temperature. This may be one of the reasons for the increase in *n* at low temperature as shown in inset of Fig. 6. The magnitude of barrier height ϕ_b of the device is 0.78 at room temperature. If we establish forward bias conditions by applying a positive voltage to the *n*-type material, the majority carrier, electrons, will be attracted to the interface,
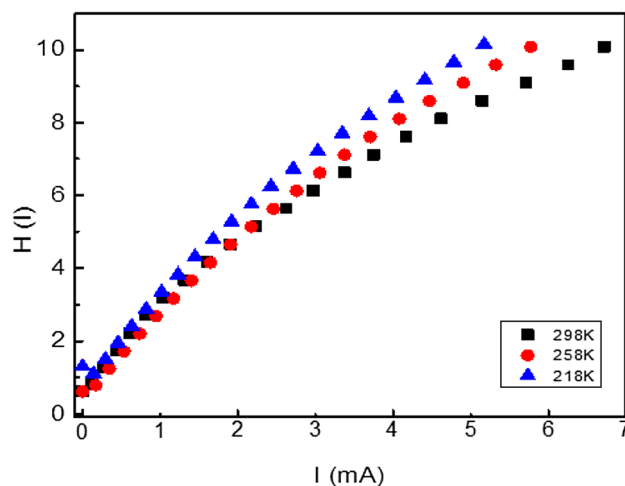
Fig. 7 Variation of H(*I*) with *I* for FTO/ZnO/PEDOT:PSS device at different temperatures in forward bias
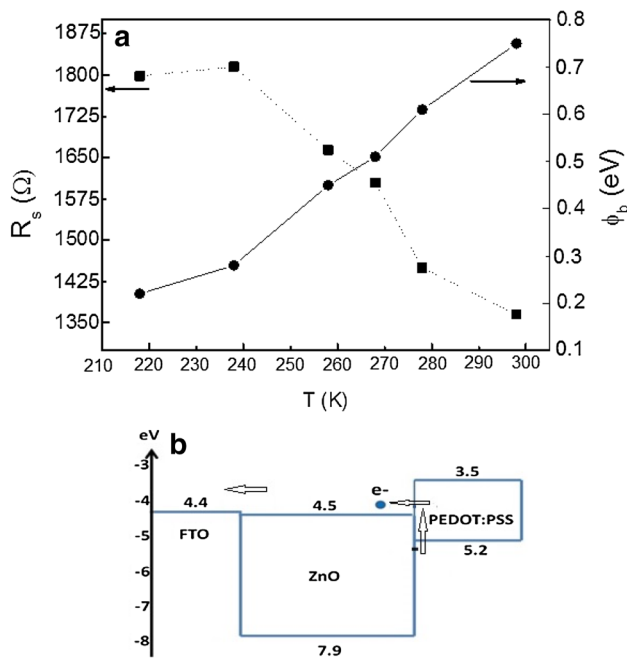
Fig. 8 **a** Variation of R_s (left axis) and barrier height (φ_b) (right axis) with temperature for FTO/ZnO/PEDOT:PSS device in forward bias obtained from H(I) function versus I plot. **b** Shows band diagram and charge transport directions inside the device

reducing the depletion width to near zero. For *p*-type materials, a negative voltage is required to accumulate majority carrier holes. To delineate carrier type behaviour, the FTO/ZnO/PEDOT:PSS device structure was fabricated with both *n*-type ZnO and *p*-type PEDOT:PSS materials. Without applying any bias, φ_b for electrons and holes are 1.1 and 5.7 eV respectively as shown in band diagram of the device in the inset of Fig. 8b. The experimental data suggest that the majority carriers in this case are electrons, which accumulate near the ZnO/PEDOT:PSS Schottky junction at room temperature. The decrease in ϕ_b with lowering the temperature may be due to an inhomogeneous barrier interface between ZnO and PEDOT:PSS. Charge carriers at low temperature are able to cross low barriers and current transport across the interface would be caused by current flowing through patches of lower Schottky barrier height [36]. The number of charge carriers with sufficient energy to overcome the barriers would be expected to increase with an increase in temperature. Therefore, current transport through lower Schottky barrier height areas and a larger ideality factor would tend to dominate device characteristics.

The presence of a possible space charge limited current (SCLC) transport mechanism in the device has also been explored. The high value of *n*, presence of large series resistance and a low zero-bias barrier height indicate that thermionic emission is not the only current transport mechanism operational at higher voltages (region II). In this region, the

behaviour of the forward bias current is typical of a SCLC transport mechanism, controlled by trap levels. The relation for the current I in this case is given by following equation [37]:

$$I \propto \left(\frac{9}{8}\right)\epsilon\epsilon_0 a\mu\frac{V^2}{d^3} \qquad (7)$$

where V is the applied voltage, μ is the carrier mobility, $\varepsilon = 9$ is the dielectric constant of ZnO, a is the active area and d is the distance between the electrodes (5169 nm). When the applied voltage is low, the current appears to be controlled by thermally generated carriers, rather than injected carriers. However, once the bias voltage is exceeded the turn-on voltage, injected carriers dominate over the thermally generated carriers. Further increases in applied voltage results in the formation of a space charge region formed from injected carriers in the bulk of wide band gap semiconductor. Further carrier injection is then inhibited by the presence of injected space charge by increasing applied voltage ($V > 3$ V), giving
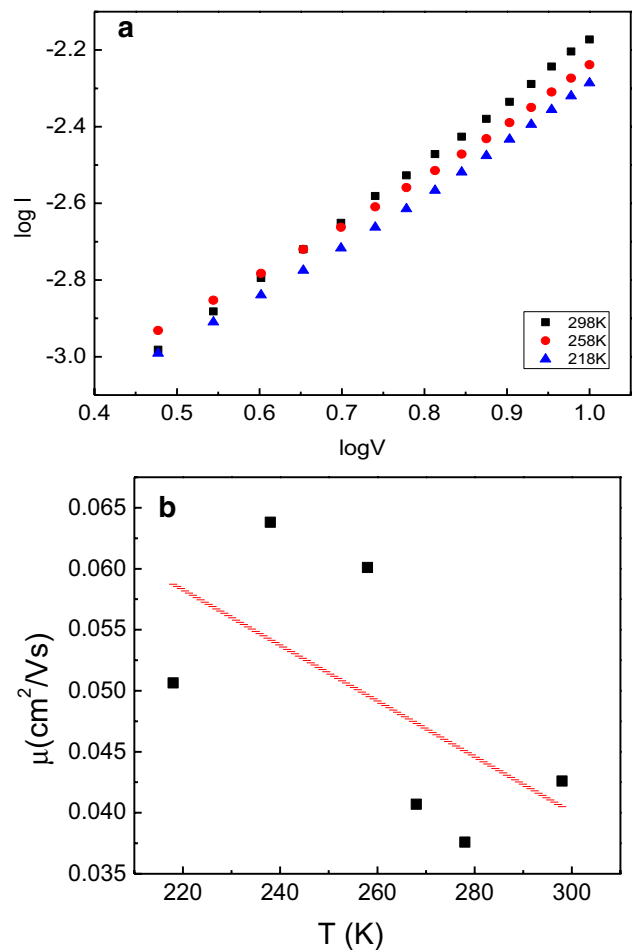

Fig. 9 **a** Variation of log I with log V plot for higher voltage region II of FTO/ZnO/PEDOT:PSS device at different temperatures. **b** Shows variation of mobility of charge carriers (μ) with temperature
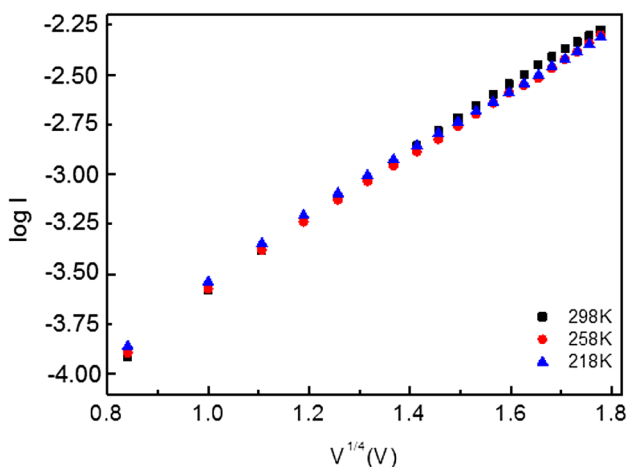
Fig. 10 Variation of log (I) with $V^{1/4}$ for FTO/ZnO/PEDOT:PSS device in reverse bias at different temperatures

rise to $I \sim V^m$ limited conduction. Charge carrier mobility μ can be estimated from Eq. 7 for the device, accounting its geometry, for all temperatures. Figure 9 shows a plot of the variation of log I with log V at different temperatures, for the higher voltage region II of the device, following Eq. 7. The maximum μ obtained, from the intercept of linear plot between log I versus 2log V at room temperature, is 0.0426 cm^2/Vs. Similar SCLC has been reported for 330 nm thick ZnO film with 10% polymethyl vinyl etheralt-maleic anhydride stabilisers on glass substrates at room temperature under atmospheric condition [38]. The inset of Fig. 9 shows the magnitude of μ decreases with an increase in temperature, which may for example be caused by changes in surface states of polymer related to specific surface groups.

I–V curves in reverse bias, as shown in Fig. 4, show a lack of saturation of the current with voltage which indicates that the Schottky barrier height may be bias dependence. There are many reasons for this dependence on image force,
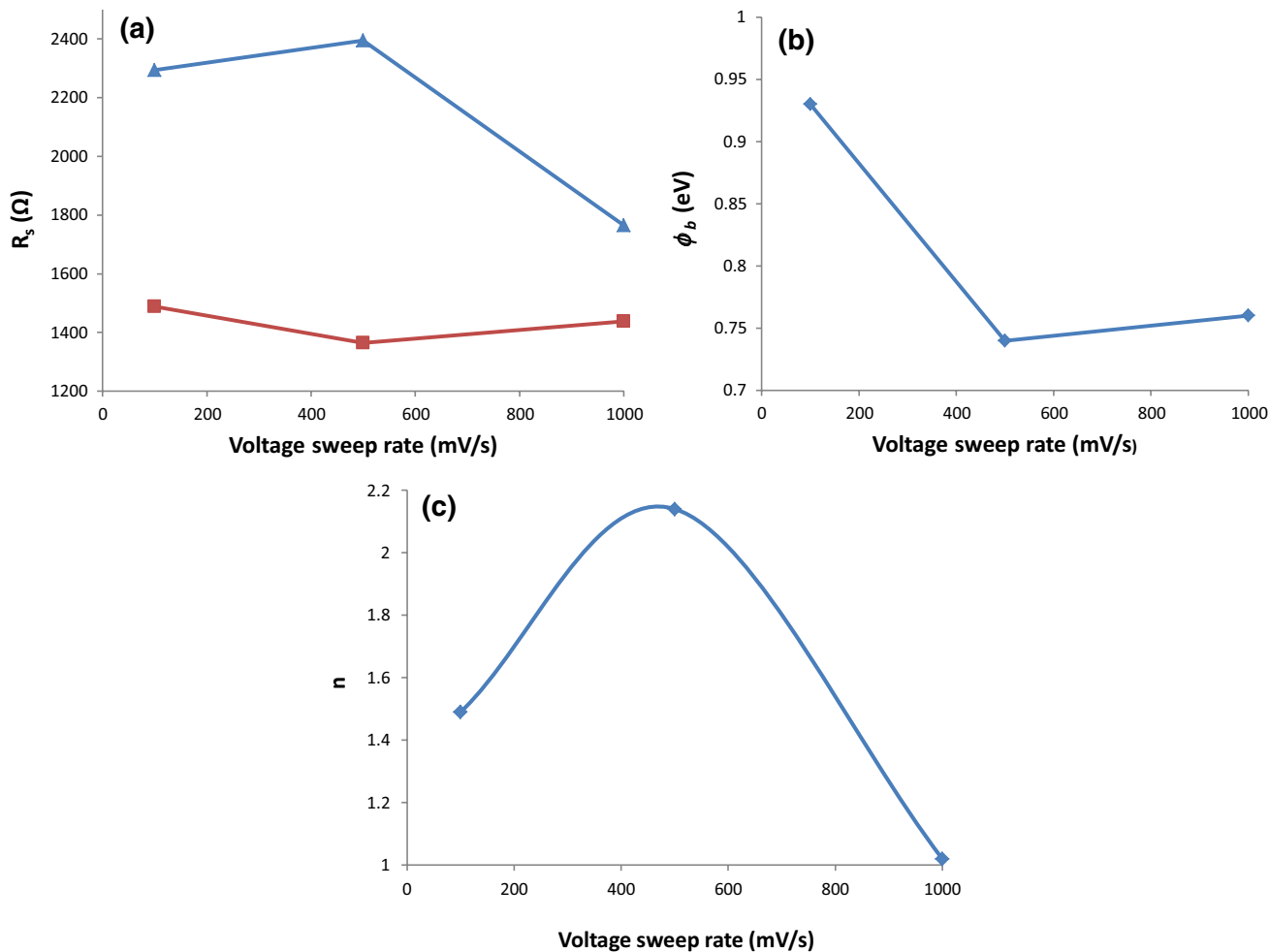
Fig. 11 a Series resistance (R_s), calculated from Equation of 4 (solid triangle) and Equation of 6 (solid square), **b** Schottky barrier height (φ_b) and **c** ideality factor (n)

interfacial layers and barrier inhomogeneities [39]. The barrier height lowering ($\Delta\phi_b$) due to image force effect alone could be checked by plotting a graph between log I versus reverse bias voltage $V_r^{1/4}$ as shown in Fig. 10. The straight line nature of this plot confirms the effect of image force on Schottky barrier height which is also supported by studies published in the literature [40]. Further measurements have been performed at room temperature to examine the effect of the scan rate on the Schottky barrier height ϕ_b, ideality factor n and series resistance R_s. The dependences of these Schottky diode parameters on the voltage sweep rate are shown in Fig. 11 as the bias voltage was swept from $+10$ to 0 V with the rate varying from 100 to 1000 mV/s. It can be seen that the diode behaviour is nearly ideal at 1000 mV/s in relative to lower scan rates. The accuracies ΔR_s in values of R_s are found to be significantly improved when Eq. (6) is used instead of Eq. (4) and ΔR_s is estimated to be small as $\pm 8\ \Omega$.

4 Conclusions

In this work, FTO/ZnO/PEDOT:PSS devices have been prepared by a simple spin-coating method. The morphological, spectroscopic and optical properties of the ZnO annealed film has been investigated with XRD, FTIR, and Photoluminescence measurements respectively. The electrical properties of this Schottky device have also been studied in depth with the help of DC I–V measurements in the temperature range of 218–298 K. Voltage sweep rate independent, hysteresis-free I–V plot shows the rectifying nature of the device which may result from the electrical nature of the components rather than from interface or contact related phenomena. The parameters such as φ_b, n, R_s of this structure have been calculated from the forward bias I–V characteristics as a function of device temperature following Cheung's method in the lower voltage region I. The value of φ_b was found to increase with increases in temperature whereas the values of n and R_s decrease with temperature. In the higher voltage region II, the SCLC conduction mechanism is applicable for the device and temperature dependent mobility values have been calculated. In summary, it has been shown that the properties of FTO/ZnO/PEDOT:PSS structures, prepared by a simple spin-coating method, are suitable for use as high-performance Schottky diode devices. Hence PEDOT:PSS could be successfully used as an alternative to expensive metal electrodes in ZnO-based inorganic semiconductor devices.

References

1. Y. Xia, K. Sun, J. Ouyang, Solution-processed metallic conducting polymer films as transparent electrode of optoelectronic devices. Adv. Mater. **24**, 2436–2440 (2012)
2. F.E. Jones, B.P. Wood, J.A. Myers, C. Daniels-Hafer, M.C. Lonergan, Current transport and the role of barrier inhomogeneities at the high barrier n-InP | poly(pyrrole) interface. J. Appl. Phys. **86**, 6431–6441 (1999)
3. S. Kee, N. Kim, B.S. Kim, S. Park, Y.H. Jang, S.H. Lee, J. Kim, J. Kim, S. Kwon, K. Lee, Controlling molecular ordering in aqueous conducting polymers using ionic liquids. Adv. Mater. **28**(39), 8625–8631 (2016). https://doi.org/10.1002/adma.201505473
4. N. Kim, S. Kee, S.H. Lee, B.H. Lee, Y.H. Kahng, Y.R. Jo, B.J. Kim, K. Lee, Highly conductive PEDOT:PSS nanofibrils induced by solution-processed crystallization. Adv Mater. **26**, 2268–2272 (2014)
5. H. Xu, R.F. Chen, Q. Sun, W.Y. Lai, Q.Q. Su, W. Huang, X.G. Liu, Recent progress in metal-organic complexes for optoelectronic applications. Chem. Soc. Rev. **43**(10), 3259–3302 (2014). https://doi.org/10.1039/c3cs60449g
6. J.Y. Kim, J.Y. Oh, S. Cheon, H. Lee, J. Lee, J.I. Lee, H. Ryu, S.M. Cho, T.Y. Kim, C.S. Ah, Y.H. Kim, C.S. Hwang, Optimized ion diffusion depth for maximizing optical contrast of environmentally friendly PEDOT:PSS electrochromic devices. Opt. Mater. Express **6**(10) 3127–3134 (2016). https://doi.org/10.1364/OME.6.003127
7. M. Cai, Z. Ye, T. Xiao, R. Liu, Y. Chen, R.W. Mayer, R. Biswas, K.-M. Ho, R. Shinar, J. Shinar, Extremely efficient indium–tin-oxide-free green phosphorescent organic light-emitting diodes. Adv. Mater. **24**, 4337–4342 (2012)
8. S.H. Park, J. Kim, C.E. Park, J. Lee, H.S. Lee, S. Lim, S.H. Kim, Optimization of electrohydrodynamic-printed organic electrodes for bottom-contact organic thin film transistors. Org. Electron. **38**, 48–54 (2016)
9. Y.F. Wang, B.Y. Jia, F. Qin, Y. Wu, W. Meng, S.X. Dai, Y.H. Zhou, X.W. Zhan, Semi-transparent, non-fullerene and flexible all-plastic solar cells. Polymer **107** 108–112 (2016)
10. C.F. Zhang, T.M. Higgins, S.H. Park, S.E. O'Brien, D.H. Long, J. Coleman, V. Nicolosi, Highly flexible and transparent solid-state supercapacitors based on RuO2/PEDOT:PSS conductive ultrathin films. Nano Energy **28**, 495–505 (2016). https://doi.org/10.1016/j.nanoen.2016.08.052
11. L.J. Brillson, Y. Lu, ZnO Schottky barriers and Ohmic contacts. J. Appl. Phys. **109**, 121301 (2011)
12. M. Nakano, A. Tsukazaki, R.Y. Gunji, K. Ueno, A. Ohtomo, T. Fukumura, M. Kawasaki, Schottky contact on a ZnO (0001) single crystal with conducting polymer. Appl. Phys. Lett. **91**, 142113 (2007)
13. M. Nakano, T. Makino, A. Tsukazaki, K. Ueno, A. Ohtomo, T. Fukumura, H. Yuji, S. Akasaka, K. Tamura, K. Nakahara, T. Tanabe, A. Kamisawa, M. Kawasaki, Transparent polymer Schottky contact for a high performance visible-blind ultraviolet photodiode based on ZnO. Appl. Phys. Lett. **93**, 123309 (2008)
14. R.Y. Gunji, M. Nakano, A. Tsukazaki, A. Ohtomo, T. Fukumura, M. Kawasaki, Polymer Schottky contact on O-polar ZnO with silane coupling agent as surface protective layer. Appl. Phys. Lett. **93**, 012104 (2008)

15. S. Paul, P.G. Harris, C. Pal, A.K. Sharma, A.K. Ray, Low cost zinc oxide for memristors with high on–off ratios. Mater. Lett. **130**, 40–42 (2014)

16. S. Paul, P.G. Harris, C. Pal, A.K. Sharma, A.K. Ray, Study of dielectric relaxation processes in printable zinc oxide films on transparent substrates. J. Mater. Sci. **26**(9) 7109–7116 (2015). https://doi.org/10.1007/s10854-015-3333-4

17. N. Hernandez-Como, A. Rodriguez-Lopez, F.J. Hernandez-Cuevas, J. Munguia, R. Garcia, R. Baca-Arroyo, M. Aleman, Current-voltage-temperature characteristics of PEDOT:PSS/ZnO thin film-based Schottky barrier diodes. Semicond. Sci. Technol. (2016). https://doi.org/10.1088/0268-1242/31/11/115007

18. J.T. Wang, X.L. Shi, W.W. Liu, X.H. Zhong, J.N. Wang, L. Pyrah, K.D. Sanderson, P.M. Ramsey, M. Hirata, K. Tsuri, Influence of preferred orientation on the electrical conductivity of fluorine-doped tin oxide films. Sci. Rep. **4**, 3679 (2014)

19. B.D. Cullity, S.R. Stock, *Elements of X-ray Diffraction*, 3rd edn. (Prentice-Hall, Englewood Cliff, 2001)

20. F.V. Molefe, L. Koao, F. Dejene, B.F. Swart H C, Phase formation of hexagonal wurtzite ZnO through decomposition of Zn(OH)(2) at various growth temperatures using CBD method. Opt. Mater. **46**, 292–298 (2015). https://doi.org/10.1016/j.optmat.2015.04.034.

21. N.G. Shimpi, S. Jain, N. Karmakar, A. Shah, D.C. Kothari, S. Mishra, Synthesis of ZnO nanopencils using wet chemical method and its investigation as LPG sensor. Appl. Surf. Sci. **390**, 17–24 (2016). https://doi.org/10.1016/j.apsusc.2016.08.050

22. S.D. Birajdar, P.P. Khirade, T.S. Saraf, R.C. Alange, K.M. Jadhav, Sol-gel auto combustion synthesis, electrical and dielectric properties of Zn1-xCoxO (0.0 <= x <= 0.36) semiconductor nanoparticles. J. Alloys Compd. **691**, 355–363 (2017). https://doi.org/10.1016/j.jallcom.2016.08.220

23. M. Benhaliliba, C.E. Benouis, M.S. Aida, F. Yakuphanoglu, A.S. Juarez, Indium and aluminium-doped ZnO thin films deposited onto FTO substrates: nanostructure, optical, photoluminescence and electrical properties. J. Sol-Gel Sci. Technol. **55**(3), 335–342 (2010)

24. K. Vanheusden, W.L. Warren, C.H. Seager, D.R. Tallant, J.A. Voigt, B.E. Gnade, Mechanisms behind green photoluminescence in zno phosphor powders. J. Appl. Phys. **79**, 7983–7990 (1996)

25. U.P. Shaik, P.A. Kumar, M.G. Krishna, S.V. Rao, Morphological manipulation of the nonlinear optical response of ZnO thin films grown by thermal evaporation. Mater. Res. Express (2014). https://doi.org/10.1088/2053-1591/1/4/046201.

26. S.D. Kshirsagar, U.P. Shaik, M.G. Krishna, S.P. Tewari, Photoluminescence study of ZnO nanowires with Zn residue. J. Lumin. **136**, 26–31 (2013)

27. G. Yip, J. Qiu, W.T. Ng, Z.H. Lu, Effect of metal contacts on the electrical characteristics of Al(2)O(3) dielectric thin films. Appl. Phys. Lett. (2008). https://doi.org/10.1063/1.2903708.

28. D.K. Schroder, *Semiconductor Material and Device Characterization*, 2nd edn. (Wiley, New York, 1998)

29. S.M. Sze, *Physics of Semiconductor Devices*, 2nd edn. (Willey, New York, 1981), pp. 7–8.

30. H.V. Wenksten, E.M. Kaidashev, M. Lorentz, H. Hochmuth, G. Biehne, J. Lenzer, V. Gottscalch, R. Pickenhain, M. Grundmann, Lateral homogeneity of Schottky contacts on *n*-type ZnO. Appl. Phys. Lett. **84**, 79 (2004)

31. S.K. Cheung, N.W. Cheung, Extraction of Schottky diode parameters from forward current-voltage characteristics. Appl. Phys. Lett. **49**, 85 (1986)

32. W. Mtangi, F.D. Auret, C. Nyamhere, P.J.J. van Rensburg, A. Chawanda, M. Diale, J.M. Nel, W.E. Meyer, The dependence of barrier height on temperature for Pd Schottky contacts on ZnO. Physica B **404**(22) 4402–4405 (2009). https://doi.org/10.1016/j.physb.2009.09.022

33. S. Yilmaz, E. Bacaksiz, İ Polat, Y. Atasoy, Fabrication and structural, electrical characterization of i-ZnO/n-ZnO nanorod homo-junctions. Curr. Appl. Phys. **12**, 1326–1333 (2012)

34. Y.-W. Song, K. Kim, J.P. Ahn, G.-E. Jang, S.Y. Lee, Physically processed Ag-doped ZnO nanowires for all-ZnO p–n diodes. Nanotechnology **20**, 275606 (2009)

35. C. Yim, N. McEvoy, G.S. Duesberg, Characterization of graphene-silicon Schottky barrier diodes using impedance spectroscopy. Appl. Phys. Lett. (2013). https://doi.org/10.1063/1.4829140

36. M.A. Yıldırım, B. Güzeldir, A. Ates, M. Sağ˘lam, Temperature dependent current–voltage characteristics of the Zn/ZnO/n-Si/Au–Sb structure with ZnO interface layer grown on n-Si substrate by SILAR method. Microelectron. Eng. **88**, 3075–3079 (2011)

37. A.K. Ray, C.A. Hogarth, A critical-review of the observed electrical-properties of MIM devices showing VCNR. Int. J. Electron. **57**(1), 1–77 (1984). https://doi.org/10.1080/00207218408938882

38. S. Bubel, N. Mechau, H. Hahn, R. Schmechel, Trap states and space charge limited current in dispersion processed zinc oxide thin films. J. Appl. Phys. **108**, 124502 (2010)

39. E.H. Rhoderick, R.H. Williams, *Metal-Semiconductor Contacts*, 2nd edn. (Oxford Science Publications, Oxford, 1988)

40. B.L. Sharma, *Metal-Semiconductor Schottky Barrier Junctions and Their Applications*. (Plenum Press, New York, 1984)